Journal of Alloys and Compounds 685 (2016) 84–90

Contents lists available at ScienceDirect

Journal of Alloys and Compounds

journal homepage: http://www.elsevier.com/locate/jalcom

The α-Fe_2O_3/g-C_3N_4 heterostructural nanocomposites with enhanced ethanol gas sensing performance

Yujing Zhang [a], Dingke Zhang [b, *], Weimeng Guo [a], Shijian Chen [a, **]

[a] School of Physics, Chongqing University, Chongqing 401331, People's Republic of China
[b] School of Physics and Electronic Engineering, Chongqing Normal University, Chongqing 401331, People's Republic of China

ARTICLE INFO

Article history:
Received 1 April 2016
Received in revised form
17 May 2016
Accepted 20 May 2016
Available online 24 May 2016

Keywords:
α-Fe_2O_3/g-C_3N_4 nanocomposites
Gas sensing
Porous nanotube
Heterojunction

ABSTRACT

The α-Fe_2O_3/g-C_3N_4 nanocomposites were synthesized by a hydrothermal and pyrolysis method. The structure and morphology of the nanocomposites were characterized by X-ray diffraction (XRD) and scanning electron microscope (SEM) techniques, which indicates porous α-Fe_2O_3 nanotubes wrapped by lamellar g-C_3N_4 structure. Due to the formation of heterojunctions, the α-Fe_2O_3/g-C_3N_4 nanocomposites demonstrate a better gas sensing performance than the pure α-Fe_2O_3 and g-C_3N_4. The α-Fe_2O_3/g-C_3N_4 heterojunctional composites with g-C_3N_4 60% weight present a maximum gas-sensing response of 7.76 toward 100 ppm ethanol at the optimum operating temperature of 340 °C, which is about 3 and 7 times higher than that of the pure α-Fe_2O_3 porous nanotubes and pure g-C_3N_4 nanopowders, respectively. Furthermore, the α-Fe_2O_3/g-C_3N_4 nanocomposites exhibit excellent selectivity to ethanol gas, faster response and recovery time than those of the pure α-Fe_2O_3 porous nanotubes and pure g-C_3N_4 powders. The possible reason for the enhanced sensing performance obtained from the α-Fe_2O_3/g-C_3N_4 nanocomposites is attributed to the porous α-Fe_2O_3 nanotubes wrapped by lamellar g-C_3N_4 nanostructures and the formation of heterojunction. The findings reported in this study will be useful to the design and construction of metal oxide nanostructures based heterojunctional structures with enhanced gas sensing performance.

1. Introduction

As the ever-growing awareness over environmental pollution and occupational safety issues, gas sensors, which play an important role in environmental monitoring, air-quality control, and detection of explosives and toxic gases, have attracted more and more research interest all over the world [1,2]. Semiconductor gas sensors based on metal oxides such as α-Fe_2O_3 [3], ZnO [4], In_2O_3 [5], SnO_2 [6], MoO_3 [7] and WO_3 [8] are the prime candidate for the sensor array owing to their tunable dimension and structures, simplicity in operation, low cost, and easy integration with electronic circuits [9]. Recently, nanocomposites have become a research hotspot for the promising applications in high-performance gas sensors. These nanocomposites have shown enhanced properties and functionalities compared to their individual metal oxide counterparts in gas-sensors due to the formation of electric junctions at the interface of the heterostructure and a more extended depletion layer [10–12].

Hematite (α-Fe_2O_3), an n-type semiconductor with a band-gap (Eg) of 2.2 eV, is particularly attractive for gas-sensing applications due to its high chemical stability, low cost, low toxicity and naturally abundant [13]. However, the efficiency of α-Fe_2O_3 is far from satisfaction due to the low responses and selectivity. Coupling α-Fe_2O_3 with other semiconductors to form heterostructure is an effective way to improve the gas-sensing efficiency. The formation of heterojunction can shorten the electron transport distance, thereby leading to the enhancement of gas-sensing efficiency [14]. On the basis of this strategy, several α-F_2O_3-based binary oxide composites such as In_2O_3/α-Fe_2O_3 [15], α-F_2O_3/NiO [16], SnO_2/α-F_2O_3 [17] and α-Fe_2O_3–ZnO–Au [18], have been reported as efficient gas sensors. It is found that the performances of these nanocomposites are closely related to their host/guest heterojunction system. For this reason, construction of α-Fe_2O_3 based heterostructure with novel guest material still has important scientific and practical significance.

* Corresponding author.
** Corresponding author.
E-mail addresses: zhangdk@cqnu.edu.cn (D. Zhang), sjchen@cqu.edu.cn (S. Chen).

http://dx.doi.org/10.1016/j.jallcom.2016.05.220
0925-8388/

Graphitic carbon nitride (g-C_3N_4), a two-dimensional (2D) planar conjugation material, has large surface area and good chemical stability [19], and most importantly, it can be easily combined with other compounds by ultrasonic dispersion method, deposition-precipitation method and so on. The g-C_3N_4 with a band gap of 2.7 eV, is suitable to implement a host/guest n/n junction architecture with α-Fe_2O_3 [20], and the conductive band of g-C_3N_4 is lower in energy than that of α-Fe_2O_3, allowing efficient electron to transport across the host/guest interface. In addition, because of its high nitrogen content, g-C_3N_4 can provide more active reaction sites than the other CN materials [21,22], and its lamellar structure benefits the transport of electron [23]. The α-Fe_2O_3/g-C_3N_4, nanocomposites have been used to supercapacitive [20], photocatalytic degradation [24] and photoelectrochemical [25] research. Thus, the combination of α-Fe_2O_3 and g-C_3N_4 is expected to be an efficient gas-sensing system. However, to our best knowledge, the investigation on α-Fe_2O_3/g-C_3N_4 nanocomposites for gas-sensing application has not been reported to date.

In this work, we developed a simple hydrothermal and pyrolysis method to prepare α-Fe_2O_3/g-C_3N_4 nanocomposites, which presented porous α-Fe_2O_3 nanotubes wrapped by lamellar g-C_3N_4 nanostructures. The resulting composites with different g-C_3N_4 mass content were used to fabricate gas sensors, aiming to demonstrate the potential applications. It was found that the gas sensor based on as-prepared α-Fe_2O_3/g-C_3N_4 heterostructural nanocomposites showed a higher response to ethanol at 340 °C, superior to the pure α-Fe_2O_3 and g-C_3N_4 individual structure. The enhanced performance had been attributed to the novel porous tubular structure as well as the change of the heterojunction barrier at the different gas atmosphere [26–28].

2. Experimental

2.1. Chemicals and materials

Ferric nitrate nonahydrate ($Fe(NO_3)_3·9H_2O$, 98.5%), melamine (C_3H_6, 98.5%), potassium hydroxide (KOH, 85%), absolute ethanol (C_2H_6O, 99.7%), and methanol (CH_4O, 99.5%) are obtained from Sinopharm Chemical Reagent Co., Ltd. All chemicals are of reagent grade and are used without further purification.

2.2. Synthesis of α-Fe_2O_3 porous nanotubes

Hematite (α-Fe_2O_3) porous nanotubes (PNs) were synthesized as follow. First, 0.01 M Fe $(NO_3)_3·9H_2O$ and 0.04 M KOH were dissolved in 10 ml deionized water, respectively. The KOH solution was then added into $Fe(NO_3)_3·9H_2O$ solution under stirring for 0.5 h. The obtained homogeneous solution was transferred into a Teflon-lined stainless-steel autoclave and kept at 100 °C for 6 h. Then the autoclave was cooled to room temperature naturally. The resultant precipitate was collected and washed by centrifugation with ethanol and deionized water several times. Then the sample dried at 60 °C in air. Finally, the α-Fe_2O_3 porous nanotubes were obtained after annealing at 600 °C for 1 h in air.

2.3. Preparation of g-C_3N_4

Graphitic carbon nitride (g-C_3N_4) powder was prepared by directly heating melamine at 550 °C in a muffle furnace for 4 h with a heating rate of 10 °C min^{-1} under air condition. The product was washed with ethanol and deionized water several times, and collected by centrifugation, and finally dried at 60 °C in air.

2.4. Synthesis of α-Fe_2O_3/g-C_3N_4 composites

In a typical procedure, a certain amount of g-C_3N_4 was added into 40 ml methanol in a beaker and ultrasonic bath for 3 h, then adding the appropriate proportion of α-Fe_2O_3 into it, and ultrasound 15 min. Then magnetically stirred at 80 °C, until the volatilization of methanol was finished, the dried product was collected. After annealing at 300 °C for 1 h in air, the α-Fe_2O_3/g-C_3N_4 nanocomposites were obtained. The specific process is shown in Fig. 1.

In this experiment, the nanocomposites with different g-C_3N_4 mass fraction were synthesized for comparison. For example, the nanocomposites, which was marked as CF-0.6, was synthesized with 0.03 g g-C_3N_4 and 0.02 g α-Fe_2O_3. Therefore, mass fraction 70%, 50%, 40% were marked as CF-0.7, CF-0.5, CF-0.4, respectively. The pure α-Fe_2O_3 and g-C_3N_4 were also synthesized by using the same processes for comparison.

2.5. Microstructure characterization

The morphology and structure of the as-synthesized samples were characterized by a field emission scanning electron microscope (FE-SEM, TESCAN MARI3) and a X-ray diffractometer using Cu Kα radiation with λ = 1.5406 Å. Specific surface data were measured by nitrogen adsorption-desorption isotherms using a Quantachrome NOVA 1000 system with all samples degassed at 100 °C prior to measurements.

2.6. Fabrication and measurement of the gas sensors

The gas sensors were fabricated usually by using a brush-coating method. Simply: the samples were mixed with a small amount of deionized water to form the pastes, which were then brushed onto the surface of alumina electrodes to form thin films (Measuring electrode is type II planar device structure, which is 13.4 mm in length, 7 mm in width, and 0.2 mm spacing in line width). The as-obtained thin films were heated at 60 °C for several hours in air before gas-sensing test. The gas-sensing properties were tested using a commercial CGS-1TP gas-sensing analysis system (Beijing Elite Tech Co., Ltd, China). The testing sensors were placed into a closed chamber with a 20 L draught capacity. The target gases (e.g., ethanol, methanol, acetone and ammonia) were injected into the testing chamber by using a micro syringe. The testing was operated at 260–380 °C with an ethanol concentration range of 100–800 ppm. The sensitivity (S) of a gas sensor based on an n-type semiconductor was defined as S=Ra/Rg, where Ra and Rg were the resistances of the sensor in air and in the target gas, respectively. The response (τ_{res}) and recovery (τ_{recov}) times were defined as the time taken by the sensor to achieve 90% of the total resistance change after the sensor was exposed to the target gas and air, respectively.

3. Results and discussion

3.1. Structure and morphology

In order to reveal the crystalline and phase structures of the prepared nanocomposites, XRD pattern of the pure g-C_3N_4, the pure α-Fe_2O_3, and the α-Fe_2O_3/g-C_3N_4 nanocomposites were measured and shown in Fig. 2. It can be seen that the g-C_3N_4 diffraction peaks are indexed to the hexagonal structure with the lattice parameters of a = 6.426 Å and c = 2.459 Å, which is consistent with the Joint Committee on Powder Diffraction Standards card (JCPDS, 50-1250). The diffraction peaks of the pristine α-Fe_2O_3 are also matched well with that of standard XRD patterns of

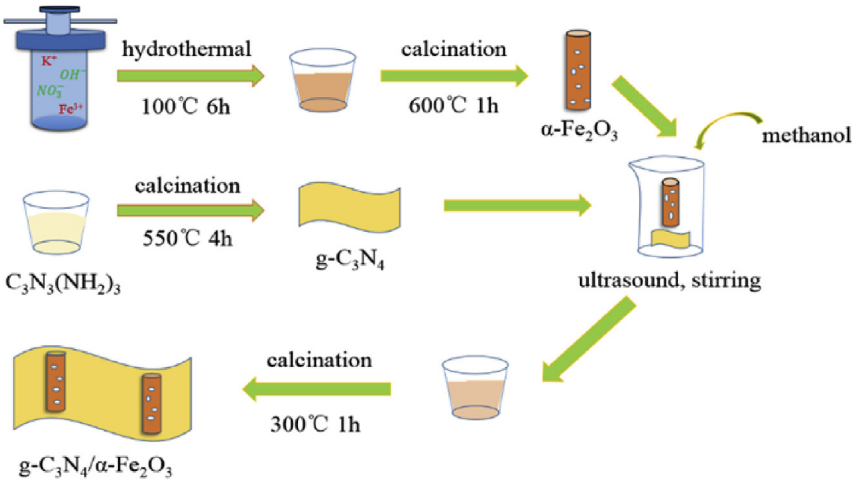

Fig. 1. Flowchart for nanocomposite samples preparation.

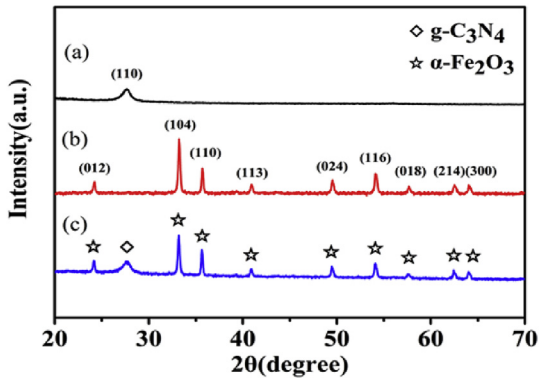

Fig. 2. XRD patterns of (a) the pure g-C_3N_4, (b) the pure α-Fe_2O_3 porous nanotube, and (c) the α-Fe_2O_3/g-C_3N_4 nanocomposites.

the rhombohedral structure of α-Fe_2O_3 with lattice constants of a = 5.039 Å and c = 13.77 Å (JCPDS card, no. 85-1327). Only reflection peaks of the corresponding components can be seen in the XRD patterns of the α-Fe_2O_3/g-C_3N_4 nanocomposites. No other impurity peaks can be detected, which indicates the final synthetic substance with high purity.

Fig. 3 shows the SEM image of α-Fe_2O_3, g-C_3N_4 and the α-Fe_2O_3/g-C_3N_4 nanocomposites, respectively. The α-Fe_2O_3 are porous tubular structures with a diameter of less than 100 nm. Such porous tubular structures enhance the surface area to volume ratio of the material and provide more active sites for gas molecules adsorbed on the materials to improve sensing properties. SEM image of g-C_3N_4 is shown in Fig. 3b, which demonstrates the lamellar structure of g-C_3N_4. It can be seen that the typical layered platelet-like morphology has been obtained, and its loose surface structure is conducive to other substances adsorption. For the α-Fe_2O_3/g-C_3N_4 nanocomposites, as shown in Fig. 3c and Fig. 3d, α-Fe_2O_3 porous nanotubes are wrapped by lamellar g-C_3N_4 structure, forming a heterojunction between them.

3.2. Gas sensing properties

The specific BET surface area (S_{BET}) of the prepared samples was investigated using adsorption-desorption measurements. The specific surface area (S_{BET}) of g-C_3N_4, α-Fe_2O_3 and α-Fe_2O_3/g-C_3N_4 are 21.487, 24.146 and 24.365 m^2/g, respectively. Due to its large surface area and the unique structures of the porous α-Fe_2O_3 nanotubes wrapped by lamellar g-C_3N_4, the α-Fe_2O_3/g-C_3N_4 nanocomposites might be advantageous for gas sensing applications [29]. Gas sensing properties based on α-Fe_2O_3/g-C_3N_4 nanocomposites are thus investigated, while the sensors made by pure α-Fe_2O_3 nanotubes and pure lamellar g-C_3N_4 are prepared as well for comparison.

The operating temperature is one of the key parameters of the gas sensor, which can govern the mobility of electrons so that it could highly influence the response of a gas sensor [30]. To determine the optimum operating temperature of the sensor, the response of α-Fe_2O_3, g-C_3N_4 and α-Fe_2O_3/g-C_3N_4 (with different mass fraction of composites) toward 100 ppm ethanol at the operating temperature ranging from 260 °C to 380 °C were tested and shown in Fig. 4 (The original data of the materials are shown in http://www.sciencedirect.com/science/article/pii/S0925838816302584 Fig. S1-S6 of Supplementary Material). It can be found that the response of pure g-C_3N_4 is nearly unchanged with the temperature increasing, while pure α-Fe_2O_3 is achieved the highest response of 2.6 at 320 °C. In contrast, the α-Fe_2O_3/g-C_3N_4 nanocomposites exhibit a rapid increase of response at different temperatures. The maximum response values of 5.4, 6.83, 7.76 and 3.02 are obtained for the CF-0.4, CF-0.5, CF-0.6 and CF-0.7 composites at 320 °C, 340 °C, 340 °C and 360 °C to 100 ppm ethanol, respectively. Obviously, the CF-0.6 nanocomposites achieve the highest response to ethanol at 340 °C, which is about 2.8 times of α-Fe_2O_3 porous nanotube and 7.1 times of pure g-C_3N_4. An appropriate amount of g-C_3N_4 in the nanocomposites is conducive to the dispersion of α-Fe_2O_3 porous nanotube and better heterojunctional structures can be formed between the two materials. If the g-C_3N_4 content excesses a certain value in the nanocomposites, it is usually bulk with small specific surface area and the active sites of adsorption oxygen and testing gas reduce, causing the degradation of gas sensor performance [23]. So, the optimum operating temperature is 340 °C.

Selecting the optimal mass fraction CF-0.6, we carried out comprehensive studies of the gas sensor properties. The responses of pure g-C_3N_4, α-Fe_2O_3 porous nanotube and the α-Fe_2O_3/g-C_3N_4 nanocomposites exposed to different ethanol concentrations at 340 °C were measured and shown in Fig. 4b (The original data of materials are shown in Figs. S7–S9 of Supplementary Material). Though the pure g-C_3N_4 exhibits a relatively low response, similar to pure α-Fe_2O_3 porous nanotube, the response of the nanocomposites increases with the concentration of ethanol increasing.

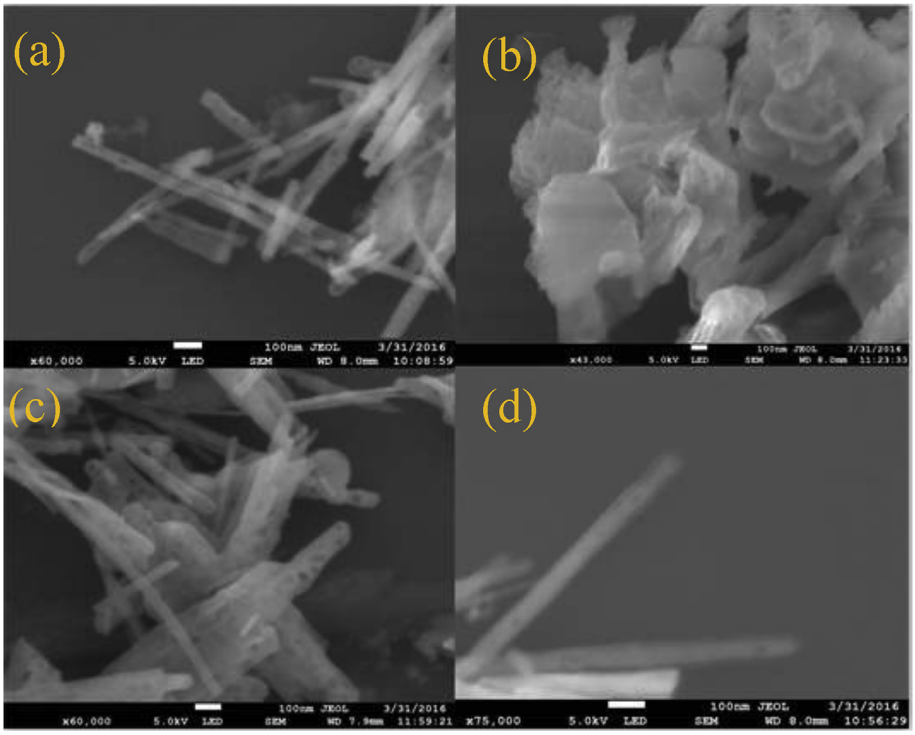

Fig. 3. Typical SEM images of as-prepared (a) α-Fe_2O_3, (b) g-C_3N_4, (c) and (d) the α-Fe_2O_3/g-C_3N_4 nanocomposites.

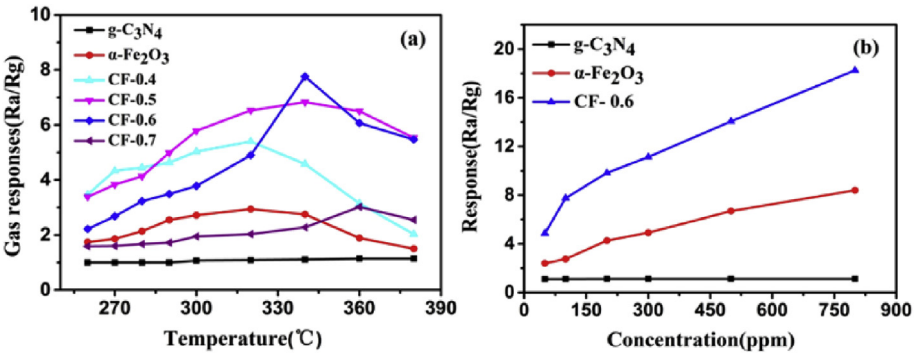

Fig. 4. (a) Responses of different gas sensors to 100 ppm ethanol as a function of the operating temperature, (b) the responses of the pure g-C_3N_4, α-Fe_2O_3, and α-Fe_2O_3/g-C_3N_4 nanocomposites (CF-0.6) versus different ethanol concentrations operating at 340 °C.

Moreover, the increase in the response depends on the gas concentrations near linearly in the range from 100 to 800 ppm for the sensor, and the slope of nanocomposites is greater than that of pure α-Fe_2O_3 porous nanotube. Obviously the sensor response has been improved due to the formation of heterojunction between the nanocomposites.

When the target gas is passed into or released, fast response and recovery time of a gas sensor usually are required in the practical application. Fig. 5a shows the dynamic response of the α-Fe_2O_3/g-C_3N_4 nanocomposites when they were exposed to 100 ppm ethanol gas at 340 °C. The almost square response shape indicates that the sensor responds rapidly to testing gas and achieves a near steady state. Then the resistance of the sensor changes slowly due to the analyze gas diffusing through the material and occupying the remaining surface reaction sites. When the sensor is exposed to air again, the resistance returns to near baseline level. The response and recovery time of the α-Fe_2O_3/g-C_3N_4 nanocomposites are 7 s and 30 s, respectively. They are shorter than the pure α-Fe_2O_3 porous nanotubes whose response and recovery time are 20 s and 33 s, as shown in the Fig. 5b. The rapid response of α-Fe_2O_3/g-C_3N_4 nanocomposites should be attributed to the heterojunctionstructures and large surface areas, providing efficient diffusion paths and adsorption sites for gas molecules.

The selectivity and stability are another two important parameters of a gas sensor in practical application. Fig. 6a shows the selectivity of the sensors based on lamellar g-C_3N_4, α-Fe_2O_3 porous nanotubes and the α-Fe_2O_3/g-C_3N_4 nanocomposites (CF-0.6) exposing to 100 ppm of several testing gases at 340 °C. In this test, gases with similar physicochemical properties, including methanol, ammonia, ethanol, and acetone, are selected for test. Obviously, the composites have a better response to ethanol than the other three gases, which is approximately 2.6–6.6 times higher than other reductive gases. In comparison, the selectivity of the pure α-Fe_2O_3 and g-C_3N_4 sensors is not as satisfactory. The excellent selectivity to ethanol is mainly due to the easier oxidation of hydroxyl group at the optimum operating temperature, which brings about the

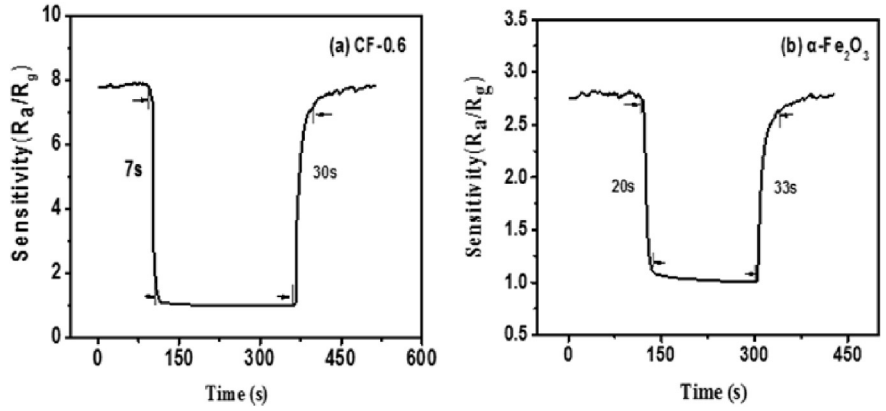

Fig. 5. Dynamic sensing response of α-Fe_2O_3/g-C_3N_4 nanocomposites (CF-0.6) and α-Fe_2O_3 nanotube to 100 ppm ethanol at 340 °C.

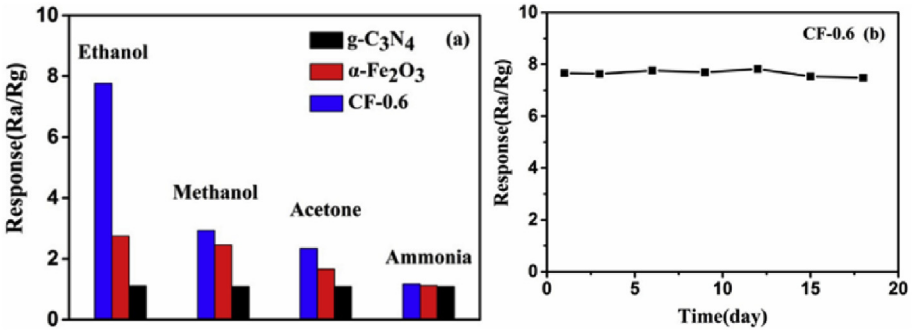

Fig. 6. (a) The selectivity of the sensors based on pure g-C_3N_4, α-Fe_2O_3 porous nanotube and the α-Fe_2O_3/g-C_3N_4 nanocomposites (CF-0.6) exposing to 100 ppm of various testing gas at 340 °C; (b) the stability evaluation of α-Fe_2O_3/g-C_3N_4 nanocomposites (CF-0.6) to 100 ppm ethanol at 340 °C.

increasing reaction between the ethanol and the absorbed oxygen [31]. Further, Fig. 6b shows the stability evaluation of α-Fe_2O_3/g-C_3N_4 nanocomposites (CF-0.6) to 100 ppm ethanol at 340 °C. It is obvious that the sensor based on α-Fe_2O_3/g-C_3N_4 nanocomposites exhibits excellent stability to 100 ppm ethanol gas at 340 °C during the 14 days of testing period. Hence, the α-Fe_2O_3/g-C_3N_4 nanocomposites have good reproducibility and stability to detect the ethanol gas.

3.3. Gas sensing mechanism

The enhanced performance observed from α-Fe_2O_3/g-C_3N_4 nanocomposites is likely to be the result of two factors. First, the α-Fe_2O_3/g-C_3N_4 nanocomposites provide large surface areas and good permeability. This means that more gas molecules can transfer to the interaction region and improve the rate for charge carriers to transverse the barriers [28]. Meanwhile, the effective and rapid gas diffusion toward both the inner and surface regions can be easily accomplished because of the porous nanotube and large lamellar nanosheet structure. Therefore, a high response and a short response time are obtained. Second, the formation of the heterojunction between α-Fe_2O_3 and g-C_3N_4 is the principal factor of the enhanced response of nanocomposites.

The sensing mechanism of the n-type semiconductor can be explained by the change in resistance of the sensor, with the chemical adsorption and desorption of gas molecules. As schematically in Fig. 7, when the n-type semiconductor is exposed to air, oxygen molecules are adsorbed on the surfaces of the sensing materials, which captures electrons from the conduction band to form oxygen ions such as O_2^-, O^- and O^{2-} [32]. With the temperature increasing, the further reaction of the oxygen ions with electrons will lead to the reduction of electron concentration, and form electron depletion layers on the surface. The reactions are as follows:

$$O_{2(gas)} \rightarrow O_{2(ads)}$$

$$O_{2\,(ads)} + e^- = O_{2\,(ads)}^- \quad T < 100^\circ C$$

$$O_{2\,(ads)}^- + e^- = 2O_{2\,(ads)}^- \quad 100^\circ C \le T \le 300^\circ C$$

$$O_{(ads)}^- + e^- = O_{2\,(ads)}^- \quad T > 300^\circ C$$

When it reaches a certain temperature, the adsorption becomes difficult, it will weaker than desorption. Thus, the point is the optimum operating temperature.

Since the n-type semiconductors electrical conductivity relies on electrons, reducing the free charge carriers concentration will lead to the upward of conduction band, and the resistance of the n-type semiconductor will increase along with the depletion region widening. When it is exposed to reducing gases, reducing gas will react with these surface oxygen ions [33]. For example, ethanol with oxygen ions reaction is as follows:

$$C_2H_5OH + O_2^-, O^-, O^{2-} \rightarrow CO_2 + H_2O + e^-$$

Electrons will be released back to the conduction band of the n-type semiconductor, then the increasing electron concentration leads to the decrease of the semiconductor resistance.

Owing to the n-type conductivity of both α-Fe_2O_3 and g-C_3N_4,

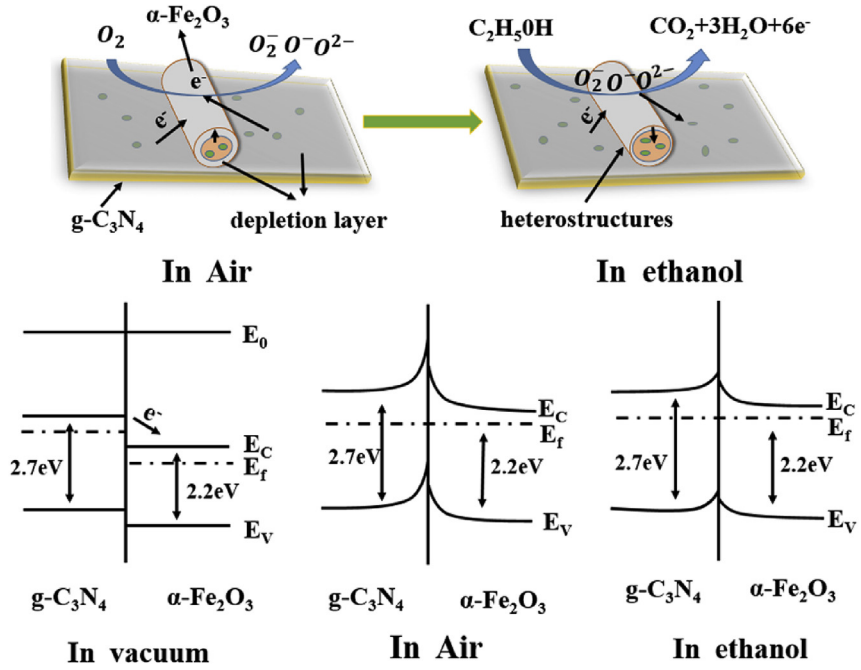

Fig. 7. The schematic diagram of test gas reaction with the as-prepared nanocomposites and the changes of the energy band in different gases.

when conduction band electrons react with oxygen molecules, the formed electron depletion layer on the surface results in an increase of the resistance (shown in Fig. 7). However, when it is exposed to ethanol gas, reaction between the oxygen ions and gas molecules will occur at the surface, which will lead to the release of electrons captured in the oxygen ions back to the conduction band of α-Fe_2O_3 and g-C_3N_4, thereby the carrier concentration increases and resistance decreases. When the α-Fe_2O_3 and g-C_3N_4 compound are combined, the heterojunction will form between the composites. Since the work function of α-Fe_2O_3 ($\Phi_{\alpha\text{-}Fe2O3} = 5.8$ eV) is larger than g-C_3N_4 ($\Phi_{g\text{-}C3N4} = 4.3$ eV), the electrons will inflow from the conduction band of g-C_3N_4 to that of α-Fe_2O_3 and lead to conduction band bent upward until the Fermi level is equal and the potential barrier becomes higher [25,28]. These heterojunction may reduce hole-electron recombination at a certain extent [34] and enable more electrons to migrate effectively from gas to the surfaces of the sensing materials when the composites are exposed to the reducing gas. Consequently, the conductivity of the heterostructure can be greatly increased, which results in a higher response.

4. Conclusions

In this work, a simple hydrothermal and pyrolysis method has been successfully explored to synthesize α-Fe_2O_3/g-C_3N_4 nanocomposites. The as-synthesized α-Fe_2O_3 and g-C_3N_4 show porous tubular and lamellar structures. The experimental results indicate that the CF-0.6 nanocomposites show a good gas sensing response to 100 ppm ethanol at the optimum operating temperature of 340 °C. Through the ethanol gas sensing test, the nanocomposites exhibit a relatively high response, good sensitivity, better selectivity, short response-recovery times and a nice stability. Therefore, the α-Fe_2O_3/g-C_3N_4 nanocomposites are promising for the practice of the detection of ethanol.

Acknowledgments

This work was supported by the National Natural Science Foundation of China (NSFC) (Grant Nos. 11304406 and 61307035), and Science and technology research Foundation of the Education Department of Chongqing Municipality (KJ1400501).

Appendix A. Supplementary data

Supplementary data related to this article can be found at http://dx.doi.org/10.1016/j.jallcom.2016.05.220.

References

[1] F. Röck, N. Barsan, U. Weimar, Electronic nose: current status and future trends, Chem. Rev. 108 (2008) 705–725.
[2] J.H. Lee, Gas sensors using hierarchical and hollow oxide nanostructures: overview, Sens. Actuators B 140 (2009) 319–336.
[3] X.L. Li, W.J. Wei, S.Z. Wang, L. Kuai, B.Y. Geng, Single-crystalline α-Fe_2O_3 oblique nanoparallelepipeds: high-yield synthesis, growth mechanism and structure enhanced gas-sensing property, Nanoscale 3 (2011) 718–724.
[4] F.L. Meng, N.N. Hou, S. Ge, B. Sun, Z. Jin, W. Shen, L.T. Kong, Z. Guo, Y.F. Sun, H. Wu, C. Wang, M.Q. Li, Flower-like hierarchical structures consisting of porous single-crystalline ZnO nanosheets and their gas sensing properties to volatile organic compounds (VOCs), J. Alloys Comp. 626 (2015) 124–130.
[5] J.J. Liu, G. Chen, Y.G. Yu, Y.L. Wu, M.J. Zhou, H.Q. Zhang, C.D. Lv, H. Qin, X. Qi, Template-free preparation of mesoporous single crystal In_2O_3 achieving superior ethanol gas sensing performance, RSC Adv. 63 (2016) 48–52.
[6] P. Sun, W. Zhao, Y. Cao, Y. Guan, Y.F. Sun, G.Y. Lu, Porous SnO_2 hierarchical nanosheets: hydrothermal preparation, growth mechanism, and gas sensing properties, CrystEngComm 13 (2011) 3718–3724.
[7] S.L. Bai, S. Chen, L.Y. Chen, K.W. Zhang, R.X. Luo, D.Q. Li, C.C. Liu, Ultrasonic synthesis of MoO_3 nanorods and their gas sensing properties, Sens. Actuators B 174 (2012) 12900–12906.
[8] C. Wang, X. Li, C.H. Feng, Y.F. Sun, G.Y. Lu, Nanosheets assembled hierarchical flower-like WO_3 nanostructures: synthesis, characterization, and their gas sensing properties, Sens. Actuators B 210 (2015) 75–81.
[9] A. Gurlo, Nanosensors: towards morphological control of gas sensing activity. SnO_2, In2O3, ZnO and WO3 case studies, Nanoscale 3 (2011) 154–165.
[10] Y.F. Wang, F.D. Qu, J. Liu, Y. Wang, J.G. Zhou, S.P. Ruan, Enhanced H_2S sensing characteristics of CuO-NiO core-shell microspheres sensors, Sens. Actuators B 209 (2015) 515–523.
[11] B. Wang, Y.D. Wang, Y.P. Lei, S. Xie, N. Wu, Y.Z. Gou, C. Han, Q. Shi, D. Fang, Vertical SnO_2 nanosheet@SiC nanofibers with hierarchical architecture for high-performance gas sensors, J. Mater. Chem. C 4 (2016) 295–304.

nanosheet@SiC.
[12] B.B. Wang, X.X. Fu, F. Liu, S.L. Shi, J.P. Cheng, X.B. Zhang, Fabrication and gas sensing properties of hollow core–shell SnO_2/α-Fe_2O_3 heterogeneous structures, J. Alloys Comp. 587 (2014) 82–89.
[13] H.J. Song, X.H. Jia, H. Qi, X.F. Yang, H. Tang, C.Y. Min, Flexible morphology-controlled synthesis of monodisperse α-Fe_2O_3 hierarchical hollow microspheres and their gas-sensing properties, J. Mater. Chem. 22 (2012) 3508–3516.
[14] D. Zhu, Y.M. Fu, W.L. Zang, Y.Y. Zhao, L.L. Xing, X.Y. Xue, Room-temperature self-powered ethanol sensor based on the piezo-surface coupling effect of heterostructured α-Fe_2O_3/ZnO nanowires, Nano Lett. 166 (2016) 288–291.
[15] C.H. Zhao, G.Z. Hang, W.H. Han, J.C. Fu, Y.M. He, Z.X. Zhang, E.Q. Xie, Electrospun In_2O_3/α-Fe_2O_3 heterostructure nanotubes for highly sensitive gas sensor applications, CrystEngComm 33 (2013) 6491–6497.
[16] C. Wang, X.Y. Cheng, X. Zhou, P. Sun, X.L. Hu, K. Shimanoe, G.Y. Lu, N. Yamazoe, Hierarchical α-Fe_2O_3/NiO composites with a hollow structure for a gas sensor, Appl. Mater. Interface 6 (2014) 12031–12037.
[17] B.B. Wang, X.X. Fu, F. Liu, S.L. Shi, J.P. Cheng, X.B. Zhang, Fabrication and gas sensing properties of hollow core–shell SnO_2/α-Fe_2O_3 heterogeneous structures, J. Alloys Comp. 587 (2014) 82–89.
[18] Y.V. Kanetia, J. Moriceaub, M. Liua, Y. Yuana, Q. Zakariaa, X.C. Jiang, Hydrothermal synthesis of ternary α-Fe_2O_3–ZnO–Au nanocomposites with high gas-sensing performance, Sens. Actuators B 209 (2015) 889–897.
[19] Y. Zheng, J. Liu, J. Liang, M. Jaroniec, S.Z. Qiao, Graphitic carbon nitride materials: controllable synthesis and applications in fuel cells and photocatalysis, Energy Environ. Sci. 5 (2012) 6717–6731.
[20] L. Xu, J.X. Xia, H. Xu, S. Yin, K. Wang, L.Y. Huang, L.G. Wang, H.M. Li, Reactable ionic liquid assisted solvothermal synthesis of graphite-like C_3N_4 hybridized α-Fe_2O_3 hollow microspheres with enhanced supercapacitive performance, J. Power Sources 245 (2014) 866–874.
[21] Y. Zheng, Y. Jiao, J. Chen, J. Liu, J. Liang, A.J. Du, W.M. Zhang, Z.H. Zhu, S.C. Smith, M. Jaroniec, G.Q. Lu, S.Z. Qiao, Nanoporous Graphitic-C_3N_4@Carbon metal-free electrocatalysts for highly efficient oxygen reduction, J. Am. Chem. Soc. 133 (2011) 20116–20119.
[22] J. Liang, Y. Zheng, J. Chen, J. Liu, D.H. Jurcakova, M. Jaroniec, S.Z. Qiao, Facile oxygen reduction on a three-dimensionally OrderedMacroporous graphitic C_3N_4/Carbon composite electrocatalyst, Angew. Chem. Int. Ed. 51 (2012) 3892–3896.
[23] C.S. Pan, J. Xu, Y.J. Wang, D. Li, Y.F. Zhu, Dramatic activity of C_3N_4/$BiPO_4$ photocatalyst with core/shell structure formed by self-assembly, Adv. Funct. Mater 22 (2012) 1518–1524.
[24] D. Xiao, K. Dai, Y. Qu, Y.P. Yin, H. Chen, Hydrothermal synthesis of α-Fe_2O_3/g-C_3N_4 composite and its efficient photocatalytic reduction of Cr(VI) under visible light, Appl. Surf. Sci. 358 (2015) 181–187.
[25] Y. Liu, Y.X. Yu, W.D Zhang, Photoelectrochemical study on charge transfer properties of nanostructured Fe_2O_3 modified by g-C_3N_4, Int. J. Hydrogen Energy 39 (2014) 9105–9113.
[26] W.W. Guo, T.M. Liu, J.X. Wang, W.J. Yu, R. Sun, Y. Chen, S. Hussain, X.H. Peng, Z.C. Wang, Hierarchical ZnO porous microspheres and their gas-sensing properties, Ceram. Int. 39 (2013) 5919–5924.
[27] Y.X. Liu, C.T. Gao, X.J. Pan, X.Y. An, Y.Z. Xie, M. Zhou, J. Song, H.L. Zhang, Z.Y. Liu, Q. Zhao, Y.H. Zhang, E.Q. Xie, Synthesis and H_2 sensing properties of aligned ZnO nanotubes, Appl. Surf. Sci. 257 (2011) 2264–2268.
[28] L.T. Ma, H.Q. Fan, H.L. Tian, J.W. Fang, X.Z. Qian, The n-ZnO/n-In_2O_3 heterojunction formed by a surface-modification and their potential barrier-control in methanal gas sensing, Sens. Actuators B 222 (2016) 508–516.
[29] L.L. Wang, T.T. Zhou, R. Zhang, Z. Lou, J.N. Deng, T. Zhang, Comparison of toluene sensing performances of zinc stannate with different morphology-based gas sensors, Sens. Actuators B 227 (2016) 448–455.
[30] C.X. Wang, L.W. Yin, L.Y. Zhang, D. Xiang, R. Gao, Metal oxide gas sensors: sensitivity and influencing factors, Sensors 10 (2010) 2088–2106.
[31] F.L. Meng, S. Ge, Y. Jia, B. Sun, Y.F. Sun, C. Wang, H. Wu, Z. Jin, M.Q. Li, Interlaced nanoflake-assembled flower-like hierarchical ZnO microspheres prepared by bisolvents and their sensing properties to ethanol, J. Alloys Comp. 632 (2015) 645–650.
[32] M.E. Franke, T.J. Koplin, U. Simon, Metal and metal oxide nanoparticles in chemiresistors: does the nanoscale matter? Small 2 (2006) 36–50.
[33] Y.B. Shen, S.K. Zhao, J.W. Ma, X.X. Chen, W. Wang, D.Z. Wei, S.L. Gao, W.G. Liu, C. Han, B.Y. Cui, Highly sensitive and selective room temperature alcohol gas sensors based on TeO_2 nanowires, J. Alloys Comp. 664 (2016) 229–234.
[34] M. Niu, F. Huang, L. Cui, P. Huang, Y. Yu, Y. Wang, Hydrothermal synthesis, structural characteristics, and enhanced photocatalysis of SnO_2/α-Fe_2O_3 semiconductor nanoheterostructures, ACS Nano 4 (2010) 681–688.